Nano Energy 131 (2024) 110380

Contents lists available at ScienceDirect

Nano Energy

journal homepage: www.elsevier.com/locate/nanoen

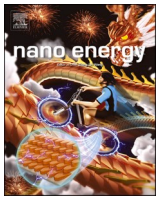

Graphene reinforced cement-based triboelectric nanogenerator for efficient energy harvesting in civil infrastructure

Wenkui Dong [a], Shanshi Gao [b], Shuhua Peng [b,*], Long Shi [c], Surendra P. Shah [d], Wengui Li [a,*]

[a] Centre for Infrastructure Engineering and Safety, School of Civil and Environmental Engineering, The University of New South Wales, NSW 2052, Australia
[b] School of Mechanical and Manufacturing Engineering, The University of New South Wales, NSW 2052, Australia
[c] State Key Laboratory of Fire Science, University of Science and Technology of China, Hefei 230026, China
[d] Center for Advanced Construction Materials, The University of Texas at Arlington, TX 76019, United States

ARTICLE INFO

Keywords:
Graphene
Self-powering
Cement-based material
Triboelectric nanogenerator
Dielectric constant
Charging performance

ABSTRACT

This paper investigated a graphene reinforced cement-based triboelectric nanogenerator (TENG) aimed at harvesting mechanical energies in infrastructure, such as pedestrians, vehicles, human-induced vibrations, and natural stimulus like wind and earthquakes. The triboelectric layers of the cement-based TENG consisted of a fully cured graphene modified cement-based plate and a polytetrafluoroethylene (PTFE) film, which were tested under a contact-separation mode. Microstructural analysis indicated that the graphene was well-dispersed in the cementitious matrix, and the graphene-cement composites achieved excellent compressive and flexural strengths of 53.0 and 3.5 MPa, respectively. The electrical characteristics of the graphene-cement composites, specifically their resistivity and impedance, showed that they did not reach the percolation threshold, making them ideal dielectric materials with a dielectric constant of 100 at 1 kHz. The performance of the cement-based triboelectric nanogenerator (TENG) varied depending on the amplitude and frequency of the contact-separation cycle. At a frequency of 10 Hz and under a force of 100 N, the short-circuit current and open-circuit voltage peaked at 3.62 μA and 279.4 V, respectively, achieving a maximum power density of 95 mW/m^2 with a 100 MΩ resistor. In practical applications, this TENG charged a 10 μF capacitor to 3.1 V within one minute and to 57.2 V in one hour. Additionally, manual operation of the TENG enabled the lighting of 29 LEDs with one minute of hand pressure. By utilizing triboelectric effects, the results provide the feasibility of self-powering concrete structures and pavements for future smart cities.

1. Introduction

Triboelectric nanogenerator (TENG) has gained increasing attention due to its simple equipment requirements, broad material selection, avoidance of chemical reactions, high sensitivity, etc. It can efficiently harness tiny mechanical energies from the environment, such as human motion, vehicle vibrations, wind, and water flow, converting these energies into electrical power [1–4]. Cement-based concrete, as one of the most widely used materials, is ubiquitous in infrastructures such as buildings, roads, bridges, tunnels, or marine structures. These structures are frequently subjected to various mechanical loadings, ranging from pedestrian, vehicular, wind, and seismic, to wave loadings [5–7]. Utilizing the principle of triboelectrification to convert the mechanical energy exerted on these cement-based concrete infrastructures into electrical energy could not only reduce the impact of unexpected loadings, enhance durability and service life, but also provide power for the lightning or sensors operation through energy harvesting.

Different materials possess varying electron affinities. When two materials come into contact and separate, electrons transfer from one material to the other, which is the mechanism behind TENG. During the friction process, materials with lower electron affinity lose electrons and become positively charged, while the counterparts with higher electron affinity gain electrons and become negatively charged [8,9]. Polytetrafluoroethylene (PTFE) has been widely used in TENG due to its highest electron affinity [10], which is followed by other polymeric materials such as polyvinylchloride (PVC), polypropylene (PP), and epoxy resin. In addition to their high electron affinity, polymers are frequently employed in TENGs as negative triboelectric layers because of their poor electrical conductivity, which inhibits electron mobility and facilitates the accumulation of charges on the surfaces. Additionally, the flexibility,

* Corresponding authors.
E-mail addresses: shuhua.peng@unsw.edu.au (S. Peng), wengui.li@unsw.edu.au (W. Li).

https://doi.org/10.1016/j.nanoen.2024.110380
Received 2 September 2024; Received in revised form 15 October 2024; Accepted 16 October 2024
Available online 18 October 2024

moldability, and biocompatibility of polymers enable their use in biomedical instruments or wearable electronic devices [11–13]. Metals (Au, Al, Cu, Fe, Al) exhibit slightly lower electron affinity compared to polymers, yet they are utilized in triboelectric nanogenerators due to several advantages. Most notably, metals possess excellent conductivity, allowing them to function effectively as electrodes in these devices [2]. For the positive triboelectric layer, the materials with lower electron affinity including paper, silk, fur, and wood are preferred. Some inorganic materials such as TiO_2, SiO_2, mica, and glass also exhibit poor electron affinity [14–17].

Cement-based composite is produced by using cement as the binder material, which is combined with well-graded sand and coarse aggregates, and then mixed with water. When cement particles come into contact with water, hydration reactions commence. These reactions proceed from the surface of the cement particles, and the main hydration products include calcium silicate hydrate (C-S-H), calcium hydroxide (CH), and ettringite (AFt) [18,19]. For incompletely hydrated concrete, it will still contain residual cement clinkers and the pores are filled with pore solutions or clinkers. To enhance the performance of concrete, including its mechanical properties, durability, and multifunctionality, nanomaterials have been widely incorporated [20–24]. The incorporation of nanomaterials, such as graphene, into cementitious materials has been shown to enhance their durability and improved resistance to chemical attacks [25], freeze-thaw cycles [26], high temperatures [27], abrasion, carbonation, reinforcement corrosion, and alkali-silica reactions [28,29]. In particular, the addition of carbon nanomaterials can improve the electrical conductivity of concrete, providing benefits such as electromagnetic interference shielding [30], piezoelectricity [31], piezoresistivity [32], and electrothermal properties [33]. Moreover, some studies have utilized carbon nanomaterials, such as nanocarbon black and graphene, to develop cement-based supercapacitors [34,35]. These innovations hold promise for directly storing electrical energy within cement-based concrete. Even though, research on the triboelectric properties of cement-based materials is scarce, which is disproportionate to their widespread use in real-life applications. Furthermore, the enhanced durability demonstrates that, as part of a smart cement-based structure, the durability of cement-based TENG far exceeds that of conventional concrete structures. Therefore, it is essential to conduct more studies in this area, which may provide a new perspective for the development of self-powered, low-carbon infrastructures and smart cities [36–38].

In this study, a new type of TENG based on graphene-modified cementitious composites and PTFE film has been developed. The cementitious materials were fully cured to ensure stable electrical output and satisfactory mechanical properties. The electrical resistivity, impedance, and relative dielectric constant of these materials were optimized to enhance power output. The performance of the cement-based TENG was evaluated in a contact-separation mode, examining the impact of both amplitude and frequency on voltage and current outputs. A manually operated TENG device was also designed to charge capacitors and power 29 LEDs. This study aims to develop a new method for creating self-powered cement-based structures and pavements, contributing to the development of sustainable and intelligent cities [39,40].

2. Materials and experimental program

2.1. Raw materials

The materials for the cement-based TENG include ordinary Portland cement (OPC), silica fume, superplasticizer, water, and graphene. The OPC is purchased from the Independent Cement & Lime Pty. Ltd., Australia. 10 % of OPC is replaced by silica fume, which is obtained from the Concrete Waterproofing Manufacturing Pty. Ltd., Australia. The polycarboxylate-based superplasticizer is produced by SIKA Australia Co., Ltd., to improve the workability of cement slurry. The lab tap water is used during the mixing. The graphene is commercially available and is obtained from the XFNANO Technology Co., Ltd., China. The specific physical, electrical and chemical properties are listed in Table 1. Based on previous studies, the addition of 1.0 % graphene by weight of binder did not reach the percolation threshold and failed to increase the conductivity greatly [41]. The mix proportion of graphene modified cement-based TENG is listed in Table 2. Additionally, the polytetrafluoroethylene (PTFE) film is introduced as another triboelectric layer with a thickness of 0.025 mm.

2.2. Preparation of cement-based TENG and testing setup

The cement-based TENG consists of cement plate and PTFE films placed in relative positions. The cement sheets are prepared from a cement paste containing well-dispersed graphene, according to the following steps shown in Fig. 1a. Initially, the graphene is added into a solution of weighted water and superplasticizer, then dispersed using a combination of ultrasonic dispersion and mechanical stirring. Subsequently, the dispersed graphene suspension is poured into a Hobart mixer, followed by the addition of cement and silica fume. The graphene cement composite is first mixed at a low speed of 140 ± 5 rpm for 1 minute, followed by mixing at a high speed of 280 ± 10 rpm for an additional 3 minutes. The well-mixed cement slurry is then cast in the mold at the size of 50 mm × 50 mm × 50 mm for compression test and 160 mm × 40 mm × 40 mm for bending test. All the specimens are cured in the curing chamber with a temperature of 25 ± 2 °C and humidity of 95 % for 28 days before conducting mechanical tests. Finally, the fully cured cement composite is cut into thin plates at 40 mm × 40 mm × 4 mm for the preparation of cement-based TENG.

The triboelectric performance of cement-based TENG is tested by a linear motor (Zaber LSQ450B-T3A), which can generate periodic contact and separation with the stroke amplitude and frequency controlled by the Zaber console software. The experimental and schematic setup to assess the triboelectric performance of cement-based TENG is displayed in Fig. 1b. The graphene-cement plate is fixed onto a metal moving bed on the U-shaped groove, with an insulating polymer board placed between them. The PTFE film is fixed to the end of the groove and is insulated by a polymer board. The copper tapes are sandwiched at the back of the cement plate and PTFE film respectively as the charge-collecting electrodes. To ensure the cement plate is fully in contact with the PTFE film, the surficial area of PTFE is slightly larger than that of cement composite reaching 50 mm^2.

2.3. Experimental program

2.3.1. Mechanical strength

The compressive and flexural strengths of graphene-cement composite are measured on the specimens at the sizes of 50 mm × 50 mm × 50 mm and 160 mm × 40 mm × 40 mm, respectively for the uniaxial compression and three-point-bending tests. The compression equipment UH500 is used at a displacement-controlled mode with rate of 0.2 mm/min for compression, and the equipment AGX50 is used with the rate of 0.1 mm/min for bending. Three duplicates are tested and averaged.

2.3.2. Water absorption and sorptivity

The water absorption and sorptivity are measured according to the standard ASTM C1585 using cylindrical specimens with the diameter of

Table 1
Physical, electrical, and chemical properties of graphene.

Appearance	Loose density (g/cm^3)	Sheets length (μm)	Layer Thickness (nm)	Carbon content	Electrical resistivity (Ω·cm)
Black powder	0.06	6–10	< 4	> 99.9 %	0.001–0.002

Table 2
Mix proportion of graphene modified cement-based TENG.

Cement	Silica fume	Water	Superplasticizer (%)	Graphene (%)
0.9	0.1	0.4	0.8	1.0

100 mm and the height of 50 mm. The water absorption can be obtained based on the Eq. (1):

$$I_t = \frac{\Delta M_t}{a \times b} \tag{1}$$

where ΔM_t is the mass changes of specimens after immersion at specific time t (s); a and b are the exposed area of specimens (mm^2) and the density of water (g/mm^3), respectively. The sorptivity is the changing rate of water absorption and obtained from the slope of water absorption. The initial sorptivity is measured within 6 hours of immersion, and the secondary sorptivity is obtained from 6 hours to the end of test.

2.3.3. Micromorphology and phase analysis

The surficial microstructures of graphene and graphene-cement composite are observed through the scanning electron microscope (SEM) and Energy-dispersive X-ray spectroscopy (EDX), to demonstrate the role of graphene in the cementitious composite. The dispersion of graphene is assessed qualitatively by an ultraviolet spectrophotometer of SHIMADZU UV-1700 with an incident light waveless of 200 nm. When the graphene suspension begins to settle, the absorbance decreases synchronously. Moreover, the milled graphene-cement powder is analyzed using X-ray diffraction (XRD) with the Bruker D8 Discover equipment.

2.3.4. Impedance and dielectric constant measurement

The resistance and impedance of the graphene-cement composite material are measured using both direct current (DC) and alternating current (AC) methods. The DC method involved directly measuring the electrical resistance using a SIGLENT SDM3045X multimeter from the time of casting to 28 days of curing. The AC method is employed to measure the impedance of the sliced cement-based triboelectric layer, utilizing an IM3536 LCR meter with a frequency ranging from 100 to 8 M Hz. The conductivity of cement-based plate can be calculated based on Eq. (2):

$$\sigma = \frac{d}{ZA} \tag{2}$$

where d is the thickness of the cement-based plate, Z is the measured impedance, and A is the cross-sectional area of cement-based plate. The capacitance of the cement-based plate can be measured by an LCR meter as well, which can be applied for the calculation of relative dielectric constant based on Eq. (3):

$$\varepsilon_r = \frac{C \bullet d}{\varepsilon_0 \bullet A} \tag{3}$$

where C is the capacitance of the cement-based plate, d is the thickness, A is the cross-sectional area and ε_0 is the permittivity of vacuum (8.854×10^{-12} F/m).

2.3.5. Triboelectric test

The triboelectric performance is evaluated by applying periodic contact and separation between the graphene-cement plate and the PTFE film using the linear motor. The force amplitude is controllable ranging from 2 to 200 N. Considering that civil engineering structures are usually subjected to low and medium frequency loads, this paper investigates the triboelectric effect of cement-based TENG under loading frequencies ranging from 1 to 10 Hz when the force of 100 N is controlled. The short-circuit current is measured through a low-noise current preamplifier (SR570, Stanford Research System), and the open-circuit voltage and current of cement-based TENG is measured by connecting a 3 GΩ resistor and the potential drop using Keithley 6514 electrometer. During the capacitor charging process by cement-based TENG, three different commercially available capacitors ranging from 10, 20–50 μF with a nominal voltage of 450 V are investigated. The digital multimeter (Keysight DMM 34465a) is used to measure the voltage of capacitor because it has a high impedance compared to the traditional multimeter [42].

3. Results and discussions

3.1. Physical, mechanical, and microstructural properties

Our previous studies have claimed that the addition of graphene in the cementitious composite could enhance the mechanical strengths and

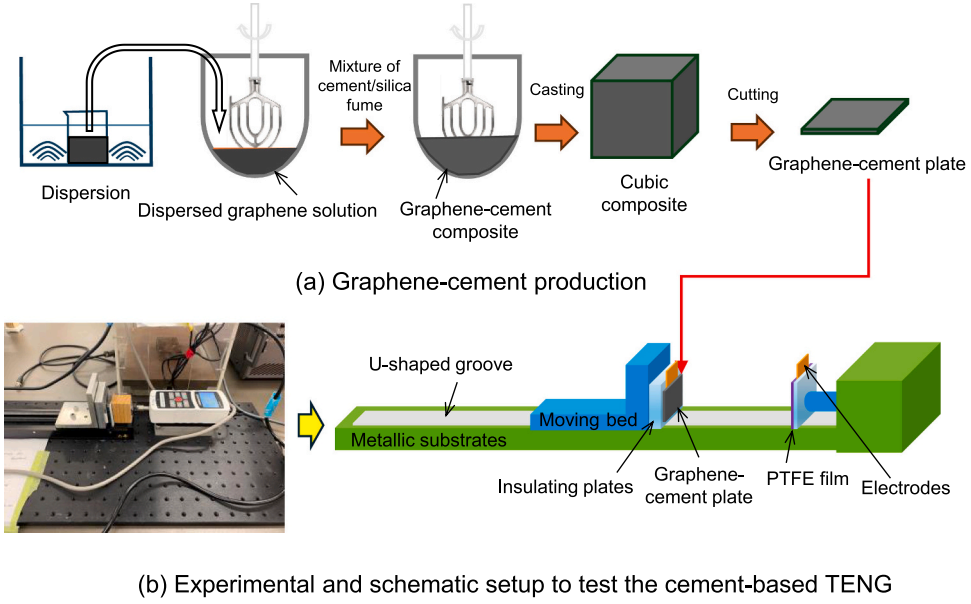

Fig. 1. Preparation procedure and experimental setup: (a) Production of graphene-cement composite; (b) Components, experimental configuration, and final product of cement-based TENG.

conductivity [43], which will not be repeated here. The physical and mechanical properties of graphene-cement composites for the preparation of cement-based TENG are investigated on their water absorption, sorptivity, compressive and flexural strengths. It could be found that the final water absorption reached nearly 4 mm after 2 days of water immersion. As shown in Fig. 2a, it can be observed that water ingression occurs rapidly during the initial stage of immersion, especially within the first 6 hours. After this period, the rate of intrusion slows down, as evidenced by the changes in sorptivity, where the initial and secondary sorptivity reached 2×10^{-2} and 2.9×10^{-3} mm•s$^{-1/2}$, respectively in Fig. 2b. The study of the water absorption and sorptivity properties of cement-based TENG is essential because cement is inherently hydrophilic and absorbs moisture from the air, which can alter its electrical properties. Therefore, excessive moisture content can increase the surficial conductivity of cement-based TENG, which may deteriorate triboelectric efficiency by neutralizing electrons [44,45]. The compressive and flexural strengths of graphene-cement composite reach approximately 53.0 and 3.5 MPa, respectively, as displayed in Fig. 2c. The mechanical strengths are higher than the ordinary cementitious materials [41], demonstrating its feasibility to be applied in engineering projects for structural or pavement construction. Moreover, the mechanical strength of cement-based TENG significantly impacts its triboelectric efficiency, primarily through improved contact effectiveness and deformation resistance. The cementitious composites with higher strengths are less prone to deformation during repeated loading and unloading cycles, ensuring better surficial contact with PTFE film. Additionally, higher mechanical strength contributes to the overall structural stability, preventing potential damages from excessive external forces.

The micromorphology of graphene is shown in Fig. 3a at different magnifications. It can be observed that the graphene used has a nanoscale thickness and a microscale width, which can serve as an effective additive for enhancing the durability and mechanical performances of cement-based materials. The thin-plate-like structure promotes cement hydration by providing nucleation sites and fills microcracks and pores within the cement, thereby inhibiting crack formation and propagation [46,47]. To achieve the benefits, it is necessary to overcome the issue of graphene agglomeration. Therefore, the combined mechanical and ultrasonic dispersion method has been proposed to disperse graphene in a water solution containing the superplasticizer. Fig. 3b shows the dispersed graphene suspension, and Fig. 3c exhibits the light absorbance of graphene suspension with standing time after the dispersion treatment. It shows that the graphene suspension has a stable absorbance in the first 50 min before slightly going down at 60 min, demonstrating the stabilized and uniformly distributed graphene in the suspension. In consideration of the mixing with cement and silica fume done in minutes, it can be deduced that the graphene is well dispersed in the matrix of cement-based TENG.

The surficial morphology, microstructures and EDX results of graphene-cement composite are shown in Figs. 3d to 3f. It is evident that the surface of the cement-based TENG has some macro pores, which are caused by the air introduced during the cement mixing process. These air pores definitely affect the contact area of cement-based TENG and also the uniform distribution of electrons [48,49]. The vibration during the casting process and the use of defoamers can help reduce the number of macro air bubbles. In a microscale, the micro pores can be observed clearly in the cement-based TENG, but the graphene is difficult to distinguish due to its nucleation effect and the attached cement hydration products (Fig. 3e). Therefore, the EDX map on carbon element is carried out to distinguish graphene from the hydration products. Even though a portion of graphene is covered by cement hydration products, the results still demonstrate that the graphene is uniformly dispersed within the cement matrix. In addition, the crystal phase composition of graphene-cement composite is illustrated by XRD analysis in Fig. 3g. It has been widely known that calcium silicate or C-S-H is the main hydration product of cement, the XRD result shows that the other main crystal compositions of cement-based TENG include the ettringite, portlandite, and the remaining OPC clinkers.

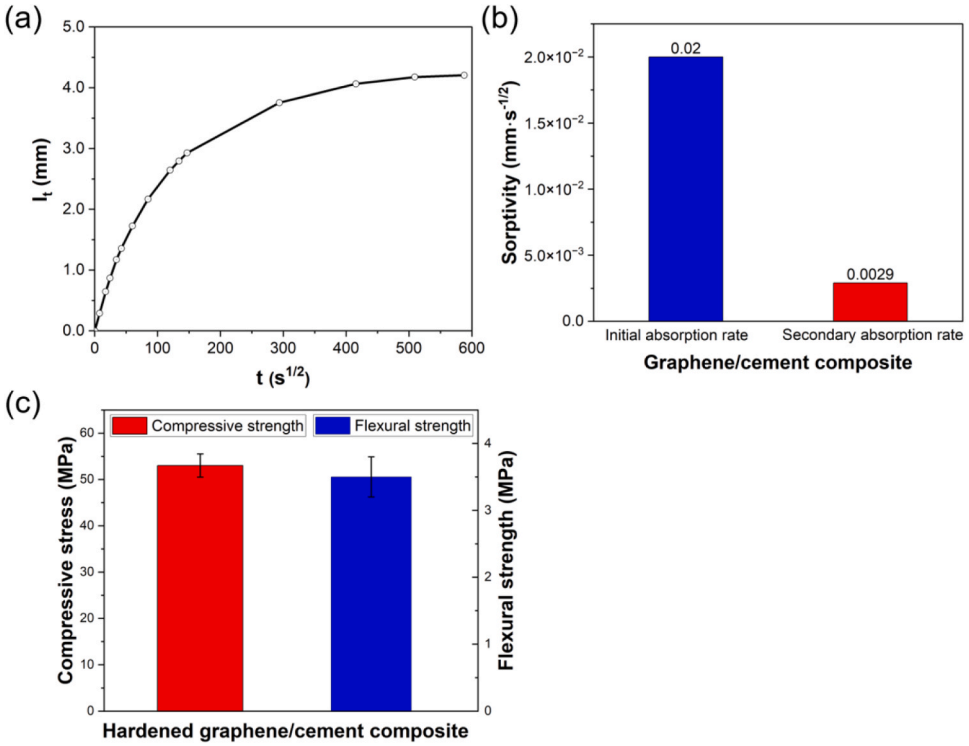

Fig. 2. The physical and mechanical properties of graphene-cement composite: (a) Water absorption; (b) First and secondary sorptivity; (c) Compressive and flexural strengths.

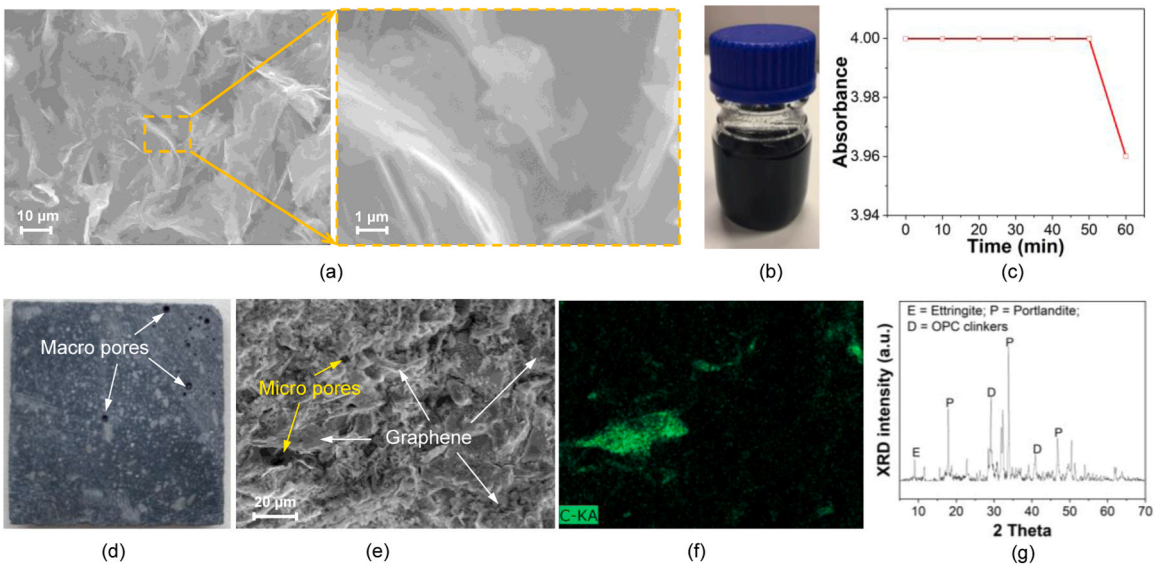

Fig. 3. Macro and micromorphology and phases: (a) Microstructures of graphene; (b) Graphene suspension; (c) Absorbance of graphene suspension; (d) Surficial morphology of cement-based TENG; (e) and (f) Microstructure and EDX results of graphene-cement composite on the element carbon; (g) XRD results of milled graphene-cement powders.

3.2. *Electrical conductivity and dielectric properties*

The electrical conductivity of cement-based composites is closely related to their hydration process. During the early stages of hydration, the high moisture content and interconnected pores result in lower electrical resistivity. As the water content decreases due to the hydration of cement clinker and the pores are gradually filled with hydration products, the resistivity tends to increase in the later curing stage, as shown in Fig. 4a. Previous studies have applied cementitious materials cured for 7 days [50,51], during which their electrical conductivity and

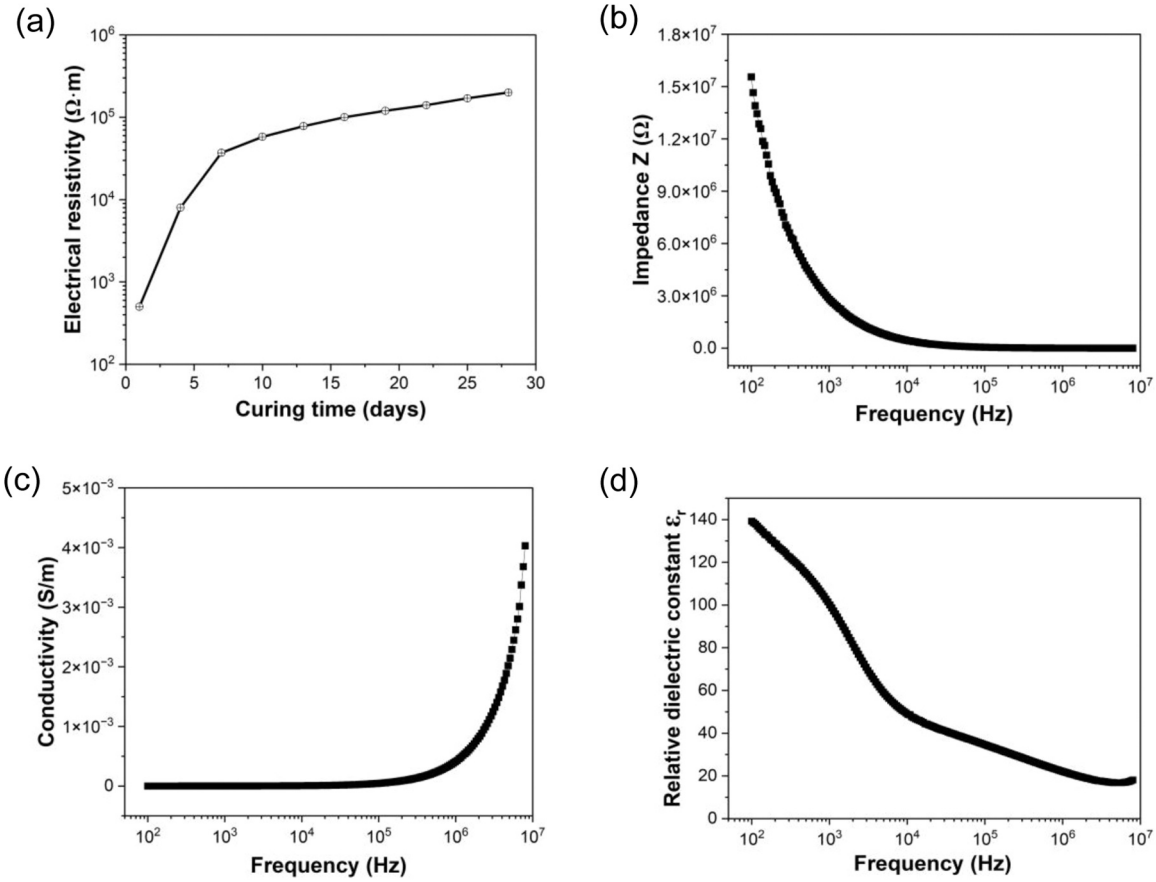

Fig. 4. Electrical and dielectric properties of graphene-cement composite: (a) Electrical resistivity development in the process of curing by DC; (b) Impedance of cement-based plate; (c) conductivity of cement-based plate; and (d) Relative dielectric constant with changing frequency.

dielectric properties may continue to change significantly with ongoing hydration. That is why the authors chose a fully cured cement matrix as a triboelectric layer, aiming to enhance the electrical stability of cement-based TENG. In terms of the impedance of cement-based plate with frequency, it rapidly decreases and then stabilizes with the increase of frequency (Fig. 4b). In the low-frequency range, the high impedance indicates the significant resistive and capacitive effects within the cementitious material. As the frequency increases, capacitive reactance decreases and leads to a decrease in impedance. In the high-frequency range, the impedance levels off, indicating that the conductive pathways in the cementitious material are well-established, and the impact of frequency on impedance diminishes. Fig. 4c illustrates the changes in electrical conductivity under varied frequencies. In the low-frequency range, the high capacitive reactance results in lower electrical conductivity. In the high-frequency range, electrical conductivity significantly increases, indicating enhanced mobility of charges in the cementitious material. The output of cement-based TENG is firmly related to the triboelectric charge density and the open-circuit voltage can be expressed by Eq. (4):

$$V_{oc} = \frac{\rho \bullet x_t}{\varepsilon_0} \tag{4}$$

where V_{oc} is the open-circuit voltage, ρ the triboelectric charge density, x_t the distance between two cement-based plates and PTFE film, and ε_o is the vacuum permittivity. The cement-based TENG in the vertical contact-separation mode can be equivalent to a capacitive model, making triboelectric charge density proportional to the capacitance the relative dielectric constant based on the Eq. (5):

$$\rho = \frac{\varepsilon_o \bullet \varepsilon_r \bullet V}{d} \tag{5}$$

where ε_r is the relative dielectric constant, d is the distance and V is the voltage drops. Fig. 4d shows the relative dielectric constant changes of cement-based plates under varied frequencies. The high dielectric constant at the low frequency indicates a strong polarization capability of the cementitious material. This is consistent with the high polarization characteristics of cement-based materials under DC conditions for the measurement of resistivity [52,53]. As the frequency increases, the polarization within the cementitious material struggles to respond timely to the changing electric field, resulting in a decrease in the relative dielectric constant. The dielectric constant of the graphene-cement plate can reach approximately 100 at the frequency of 1 kHz. This is comparable to similar studies on the TiO_2 modified cement-based triboelectric layer and the one reinforced with carbon black, in which the relative dielectric constants of 79.3 and 82.2 were obtained, respectively [50,51].

3.3. Output performance of cement-based TENG

The frequency of external loads experienced by civil infrastructure depends on the specific type of loading and environmental factors, which is usually within 10 Hz. Therefore, this section examines the impact of different loading frequencies, ranging from 1 Hz to 10 Hz, on the triboelectric efficiency of cement-based TENG under the same loading conditions of 100 N. As shown in Fig. 5a, the results show that the open-circuit current reached around 0.44 μA at the frequency of 1 Hz, and then gradually increased with the growth of frequency. The averaged short-circuit currents of cement-based TENG at the frequencies of 2, 4, and 8 Hz were 0.81, 1.68, and 3.39 μA, respectively, and rose up to the highest of 3.62 μA at 10 Hz. These are comparable to the previous studies on the cement-based TENG prepared by 7 days cured carbon black-cement composites and the PTFE sheets [51]. The open-circuit voltage of cement-based sensors was measured by the potential drop of connecting a 3 GΩ resistor. As displayed in Fig. 5b, the output voltage at 1 Hz was 72.5 V, which surged to 279.4 V at 10 Hz. It could be deduced that higher frequencies led to faster generation and accumulation of charges, resulting in an enhancement in electrostatic induction and increasing the output current [54,55]. However, it is also evident that as the frequency continues to increase, the rate of voltage growth slows down (Fig. 5c). This phenomenon is mainly due to the surface charge density of the cement-based material. Once the surface charge density reaches its peak, further increasing the loading frequency does not result in higher voltage [56,57].

Concrete infrastructure has a long-life span of decades; hence, the long-term stability ensures consistent performance over extended periods, which is crucial for practical applications of cement-based TENG. Fig. 5d shows the open-circuit voltage output of cement-based TENG

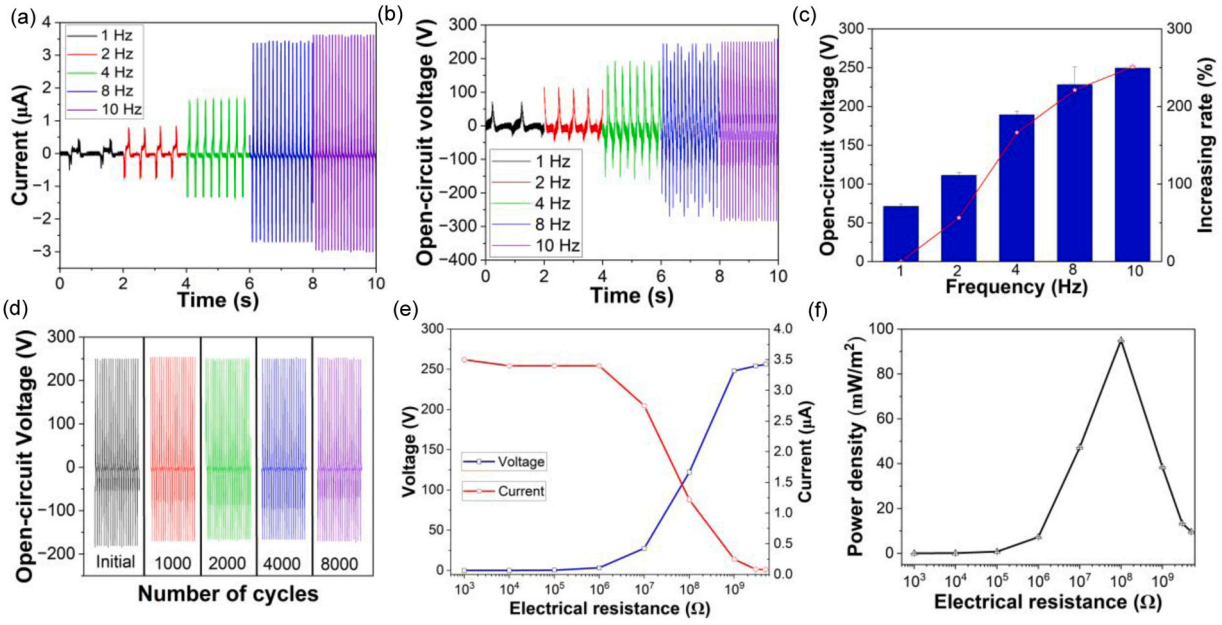

Fig. 5. Triboelectric performance of cement-based TENG under the force of 100 N: (a) short-circuit current in varied frequency from 1 to 10 Hz; (b) open-circuit voltage in varied frequency with 3 GΩ resistor; (c) voltage to frequency; (d) stability after thousands of cycles; (e) and (f) cement-based TENG output voltage, current and power density at different load resistance values.

initially, and after being subjected to 1000, 2000, 4000, and 8000 loading cycles. The results indicated that the voltage output was consistent and unchanged after thousands of loading cycles, as well as maintaining excellent repeatability and reversibility. Based on the understanding of cementitious materials, the repeatability of its electrical signals within the elastic range can be anticipated, as inferred from the author's previous research on piezoresistive cement-based sensors [58]. The loading applied in the cement-based TENG is 100 N (or 62.5 kPa), which is significantly smaller than the mechanical strength of the graphene-cement composite and within the elastic range of the cement matrix. Therefore, in this study, it can be considered that the cement-based TENG performs elastically during the loading cycles, and forces within the elastic range do not affect its long-term stability greatly.

The power density is evaluated by measuring the output voltage and current of the cement-based TENG connected to a series of resistors ranging from 1 kΩ, 10 kΩ, 100 kΩ, 1 MΩ, 10 MΩ, 100 MΩ, 1 GΩ, 3 GΩ, and 5 GΩ under a consistent impact force of 100 N at the frequency of 10 Hz. As exhibited in Figs. 5e and 5f, the voltage increased and current decreased with the increase of resistance, and the power calculated based on the equation $P = U \times I$ had a maximal value reaching approximately 151.5 μW with the power density of 95 mW/m^2 as the electrical resistance of the resistor reached 100 MΩ. In the studies by Ra et al. [59], who directly deposited the polyvinylidene difluoride-trifluoroethylene (PVDF-TrFE) nanofibrous mat onto cement composite by electrostatic spinning, the maximum power generated was 60.9 μW with the surficial contact area of 50 × 50 mm^2, which is only a quarter of the graphene modified cement-based TENG proposed in this study. Moreover, the power density of this study is comparable to the studies by Kuntharin et al. [51]. They proposed a carbon black modified cement-based TENG and achieved a high-power density of 2.13 W/m^2. However, the current they measured for power density assessment (higher than 160 μA) was much higher than the short-circuit current (around 3 μA), which may be influenced by external variables that were not fully controlled. Secondly, all the voltages and currents for the power calculation were measured from peak to peak in their studies, which may be another reason for the high power density. Overall, in consideration of the large-scale characteristics of concrete infrastructure, such as highways and buildings, the total amount of electrical energy generated by the cement-based TENG would be substantial.

The impact of force on the triboelectric efficiency of cement-based TENG is also investigated in this paper. Figs. 6a to 6c show the open-circuit voltage and short-circuit current outputs of the cement-based TENG subjected to 2, 5, 10, 50, 100, and 200 N. It shows that the voltage output increased from around 55–311 V with the increase of force applied. This is owing to the increase of force that raises the contact area between the graphene-cement plate and PTFE film, thus increasing the amount of charge accumulation and electrostatic induction to enhance output voltage [49,60]. Fig. 6b displays the short-circuit current of cement-based TENG subjected to the force of 200 N, with an average value of approximately 3.98 μA at 10 Hz. Compared to the counterpart loaded by 100 N force, the enhancement in current is not significant and that is why we decided to use 100 N to investigate the effect of frequency and power density measurement. Fig. 6c demonstrates the relationship between the voltage and current output to the compressive stress on the graphene-cement plate. Also, it can be observed that the voltage output varies significantly with changes in small force. However, as the force increases, the magnitude of these variations diminishes. The reason is due to the influence of load tends to saturate after reaching a certain level [61,62]. It can be estimated that the excessive force may damage the surficial microstructures of cement-based TENG, potentially causing plastic deformation and reducing triboelectric efficiency.

3.4. Charging properties

The electrical output of cement-based TENG can be applied to charge energy storage devices like capacitors or power electronic devices such as LEDs. Fig. 7a depicts the circuit in which a cement-based TENG is used to charge three capacitors with different capacitances: 10, 20, and 50 μF. The cement-based TENG was subjected to 100 N at a frequency of 10 Hz. A bridge rectifier was employed to convert the generated AC to DC output, before connecting to the capacitors. Fig. 7b shows the rectified open-circuit current of cement-based TENG after connecting to a bridge rectifier. The negative half-cycle of the AC signal was converted into a continuous positive voltage, with an output frequency that was twice of the original AC signal. Compared to the short-circuit current of the cement-based TENG, the current magnitude slightly decreased after passing through the rectifier. In terms of capacitor charging efficiency, the results show that within one minute, the capacitors were charged to 3.1, 1.8, and 1.0 V, respectively for 10, 20 and 50 μF capacitors (Fig. 7c). After five minutes, the voltages further increased to 13.0, 8.1, and 4.5 V. It is apparent that the voltage increased rapidly in the initial charging period, then gradually slowed down as the voltage increased. This occurs because the voltage generated by the cement-based TENG and the voltage difference across the capacitor decrease, resulting in a reduced charging current. After one hour of charging, the voltages reached 57.2, 44.6, and 24.5 V, respectively, and the subsequent growth became gentler. According to the Eq. (6):

$$E = 1/2CV^2 \tag{6}$$

Where E is the energy (J), C is the capacitance (F) and V is the voltage of the capacitor (V). Fig. 7d illustrates the charging energy of capacitors over time. Initially, the 10 μF capacitor exhibited the highest energy, but around 15 minutes, it was surpassed by the 20 μF capacitor. It indicates that despite having a higher charging voltage, a smaller capacitor does not necessarily result in better charging energy.

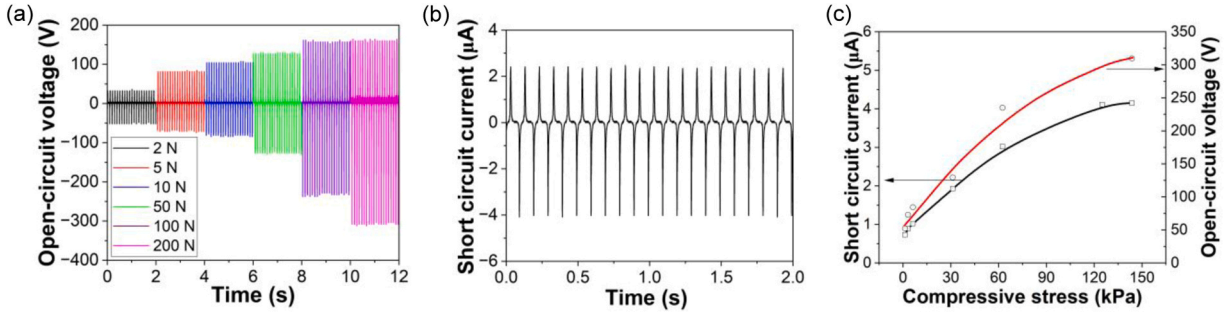

Fig. 6. Effect of force amplitude on the open-circuit voltage and short-circuit current output: (a) Voltage output under 2, 5, 10, 50, 100 and 200 N; (b) Short-circuit current under 200 N; and (c) Voltage and current output as a function to pressure.

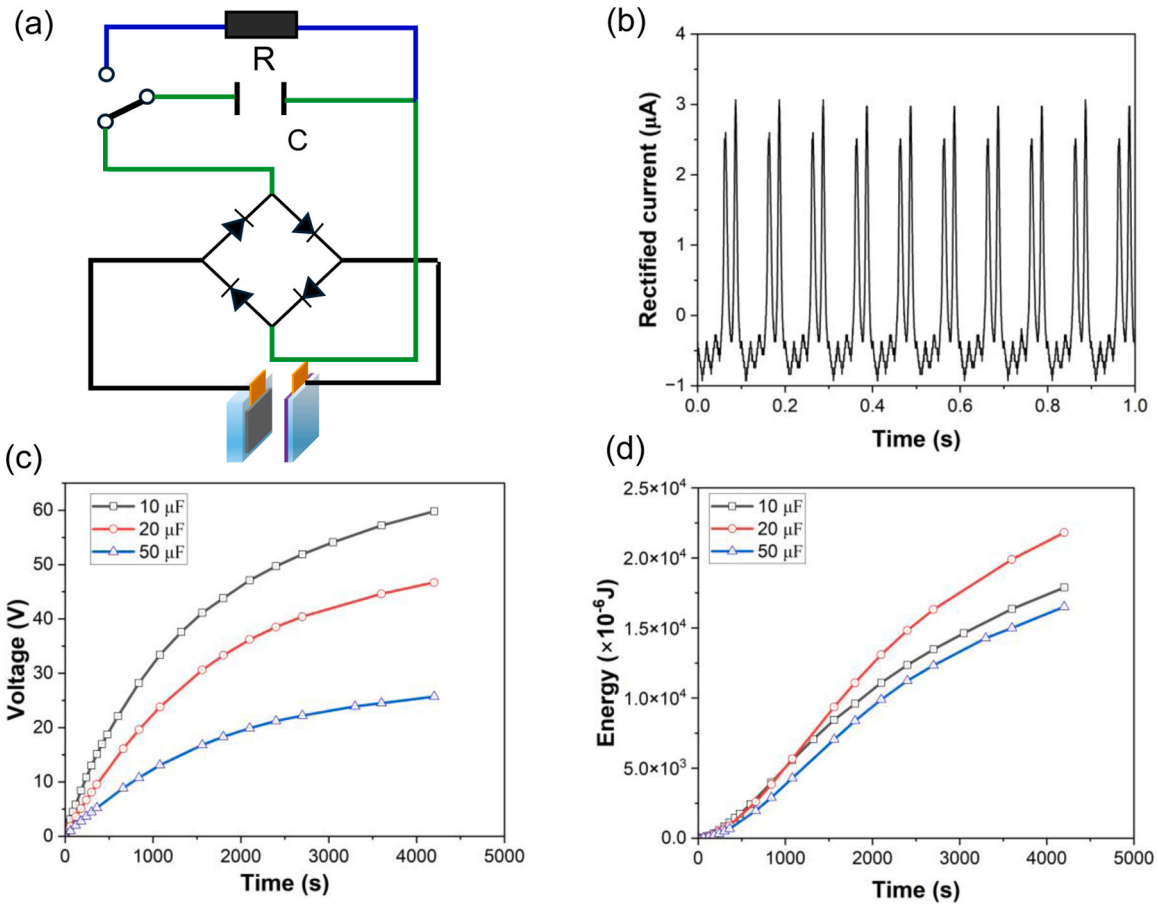

Fig. 7. Charging performance of cement-based TENG: (a) Circuit diagram to charge capacitors; (b) rectified short-circuit current; (c) and (d) Voltage and energy profiles of 10, 20, and 50 μF capacitors being charged by the cement-based TENG.

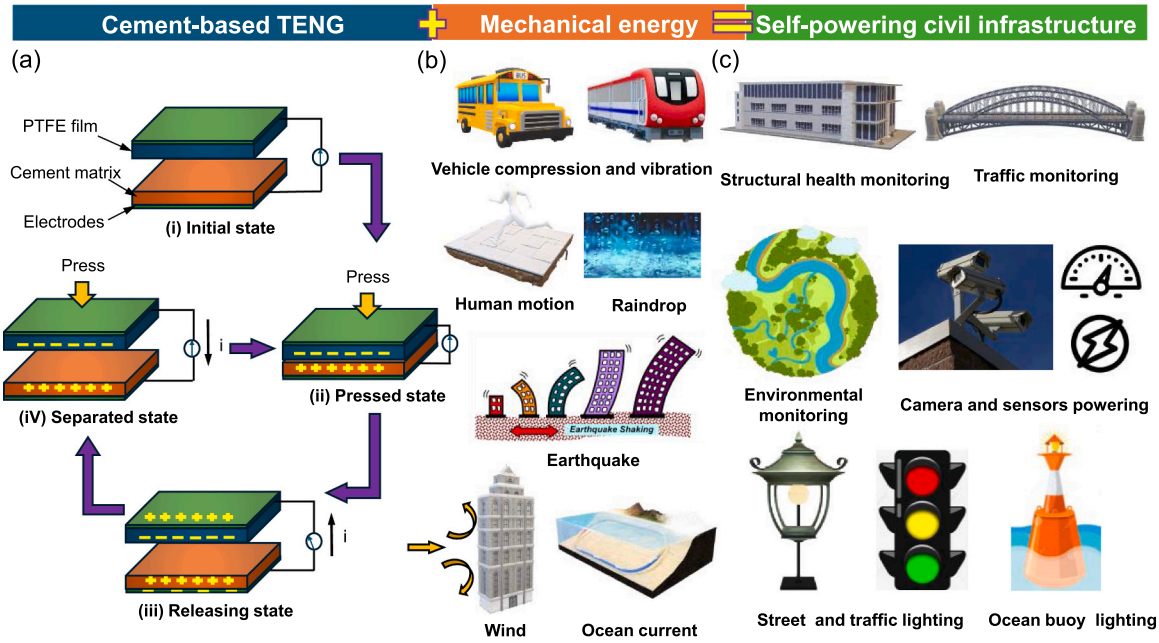

Fig. 8. Cement-based TENG for energy harvesting and multifunctional applications: (a) Triboelectric mechanism; (b) Mechanical energy existed in infrastructures; (c) Potential applications in various infrastructures.

3.5. Mechanism and applications in civil engineering

3.5.1. Mechanism and application potentials

Figs. 8a-i to 8a-iv show the schematic diagram of electron generation out of triboelectric effect and the electrostatic induction of cement-based TENG in the process of periodic contact and separation. The cement-based TENG is tested by a vertical contact and separation mode with copper tapes attached as electrodes. When the graphene-cement surface encounters the PTFE film under compression, electrons transfer from the cementitious surface to the PTFE film due to the higher electron affinity of PTFE. The results in the cementitious surface becoming positively charged and the PTFE surface becoming negatively charged with an equal number of charges. Due to the high electrical insulation properties of both the cement matrix and PTFE film, these charges accumulate on the surfaces until the maximum charge density that these two triboelectric layers can withstand is reached. It is noteworthy that the maximum charge density of the material is not affected by the loading frequency or the magnitude of stress. Therefore, theoretically, when the cement-based TENG is fully charged, increasing the load frequency and amplitude does not impact the output voltage [63]. As shown in Fig. 8a-iii, the output electrical signal is primarily due to the electrostatic induction. The negatively charged PTFE film repels electrons in the copper electrode, while the positively charged cement matrix attracts electrons, causing them to flow toward the copper electrode connected to the cement matrix. In particular, the contact and separation of two layers still cause the voltage to vary with the distance between them. When the electrodes are compressed, the distance between them decreases, leading to a reduction in voltage. Conversely, when the electrodes are separated, the distance increases, causing the voltage to rise. The contact and separation processes in this vertical loading mode cause periodic changes in the electric field, resulting in alternating positive and negative voltage peaks in the output.

As shown in Fig. 8b, civil infrastructure is frequently subjected to various external loads, ranging from artificial loads like pedestrians, vehicles, and various human-induced vibrations to natural forces such as raindrops, tide and ocean currents, wind, and earthquakes. Prolonged exposure to these loads typically results in varying degrees of structural or pavement damage. However, the application of cement-based TENG holds promise for capturing this mechanical energy and converting it into electrical energy through triboelectric and electrostatic induction effects. This process helps to harness mechanical energy but also mitigates the impact of these loads on the infrastructure, thereby extending its service life. In particular, the cement-based TENG can function as sensors by monitoring changes in electrical signals, making them feasible for structural health and traffic monitoring [64]. Additionally, they can be employed in drainage systems to monitor water quality parameters such as pH levels in real-time, as well as for air quality and road surface exhaust monitoring [65,66]. More importantly, as shown in Fig. 8c, these cement-based TENG can provide a continuous power supply to civil infrastructure. For instance, the vibration energy generated by vehicles on the road can be converted into electrical energy to power road surveillance cameras and other sensors. They also have the potential to supply power to streetlights and traffic signals. Furthermore, the mechanical energy from ocean currents and tides can be harnessed by cement-based TENG in coastal or offshore engineering applications such as digue and offshore drilling platforms.

3.5.2. Application demonstrations

A manually operated cement-based TENG was designed in the lab to demonstrate its potential application in traffic or structural infrastructures, as shown in Figs. 9a and 9b. In addition to the triboelectric layers and electrodes, the device contains four elastic foam pieces and two acrylic substrates. The circuit to charge the capacitor is identical to the aforementioned with a bridge rectifier. Hence, each manual press and release cycle brings the cement-based plate into contact with and then separates it from the PTFE film. Fig. 9c illustrates the current output of the cement-based TENG device at both low and high frequencies, as well as the current output after rectification. Uneven distribution of manual force on the cement-based TENG can result in local pressure exceeding that applied by the linear motor, which may explain why the short-circuit current is observed to be higher than that under automatic loading conditions. Fig. 9d shows the voltages of the capacitor charged by manually pressing. It can be observed that high-speed manual pressing of the cement-based TENG device can charge the capacitor to nearly 4.6 V within 2 minutes, which could light up 29 LEDs where four different colors of LEDs made up the letter 'CEMT' (Fig. 9e). It indicates that the energy generated by cement-based TENG is sufficient to power small electronics for application.

Fig. 10 demonstrates the application of cement-based TENG in civil engineering structures and pavements for energy harvesting. The two

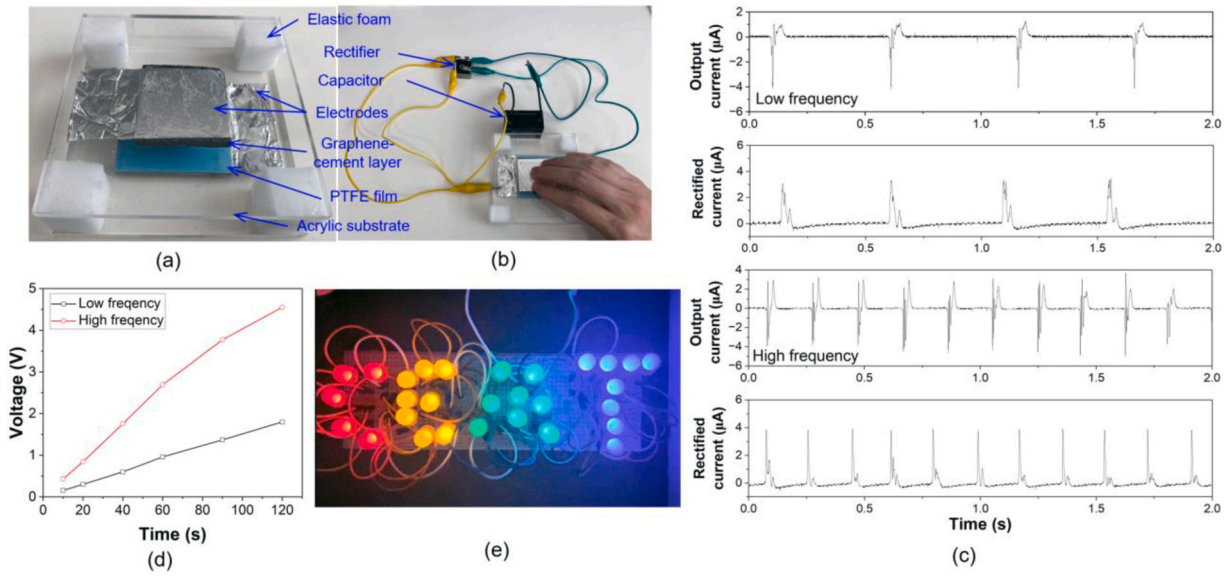

Fig. 9. Cement-based TENG designed in the lab: (a) Hand-operated cement-based TENG device; (b) Capacitor charged by the hand-operated cement-based TENG; (c) Output current and rectified current of hand-operated cement-based TENG at low and high frequencies; (d) Voltage increase of charged 10 μF capacitor; (e) Photograph displaying the letters "CEMT" by 29 LEDs light up by cement-based TENG.

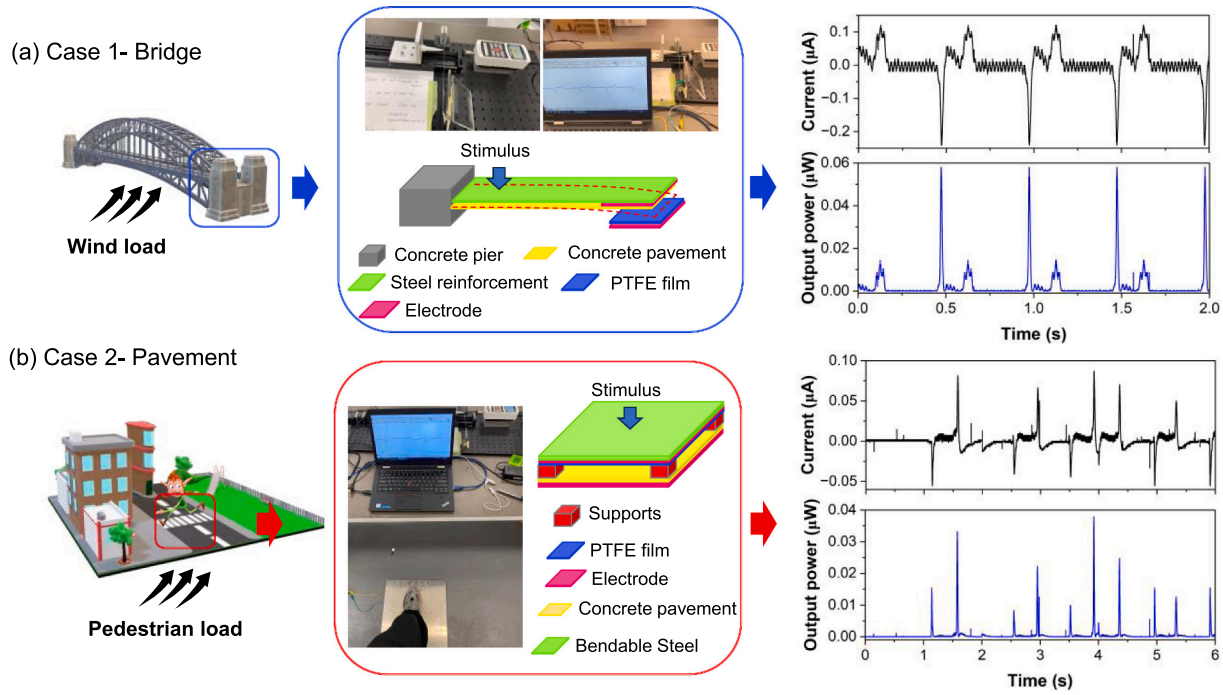

Fig. 10. Cement-based TENG designed for civil engineering application: the schematics, experimental setup and output current and power for the case 1- bridge application for wind energy harvesting and case 2- pavement application for pedestrian and vehicle induced mechanical energy harvesting.

cases presented are wind energy harvesting in bridges and mechanical energy harvesting in pavements due to pedestrian and vehicle-induced loads. The wind induces vibrations in the bridge, which act as a mechanical stimulus (Fig. 10a). The experimental setup simulates the bridge's response to wind-induced vibrations, incorporating a layered structure comprising a concrete pier, steel reinforcement, concrete pavement, PTFE film, and electrodes. The output current and power showed that the bridge application can generate an alternating current corresponding to the wind-induced mechanical oscillation (see S1). The peak output current reaches higher than 0.2 μA, and the maximum power output is around 0.06 μW (37.5 μW/m^2). In the second case, the setup involves a concrete pavement, bendable steel, PTFE film, electrodes, and supportive layers (Fig. 10b). The output current and power indicated an alternating current with peaks of about 0.08 μA and a corresponding maximum power output of approximately 0.04 μW (25.0 μW/m^2, see S2). Both cases illustrate the potential of cement-based TENG to be integrated into civil structures, providing a sustainable and self-powered solution for powering sensors or other low-power devices such as for structural health monitoring, lighting, or powering small electronic devices in smart cities.

4. Conclusions

Based on triboelectrification, this paper proposed a new cement-based TENG fabricated from the cement-based plate and the PTFE film. The related conclusions are drawn as follows:

(1) The cement-based plate was prepared from the graphene modified cementitious composite, which was fully cured for 28 days to achieve satisfactory mechanical properties and water repellency.
(2) The addition of 1.0 % graphene by weight of binder failed to enhance the conductivity of cementitious composite, while the dielectric constant of graphene cement-based plate could reach up to 100 at the frequency of 1 kHz. Both the amplitude and frequency of loading cycle impacted the voltage and current outputs. The short-circuit current reached 3.62 μA and the open-circuit voltage reached up to 279.4 V at the frequency of 10 Hz under 100 N periodic cycles.
(3) The cement-based TENG showed stabilized voltage output after being subjected to 8000 periodic cycles. The maximum power approximately 151.5 μW or the power density of 95 mW/m^2 occurred when connected to the 100 MΩ resistor.
(4) In terms of the charging performance, the cement-based TENG can charge a 10 μF capacitor to 3.1 V in a minute and 57.2 V in an hour. In addition, the manually operated cement-based TENG device could light up 29 LEDs with a minute hand press.
(5) The case studies showed that the cement-based TENG shows excellent energy harvesting capabilities in bridge and pavement for wind energy harvesting and pedestrian/vehicle induced mechanical energy harvesting, which is promising for the practical application in self-powering infrastructures.

CRediT authorship contribution statement

Shanshi Gao: Writing – review & editing, Writing – original draft, Methodology, Data curation. **Shuhua Peng:** Writing – review & editing, Writing – original draft, Validation, Resources, Methodology, Formal analysis. **Long Shi:** Writing – review & editing, Validation. **Wengui Li:** Writing – review & editing, Writing – original draft, Validation, Supervision, Resources, Funding acquisition, Conceptualization. **Surendra P. Shah:** Validation, Writing – review & editing. **Wenkui Dong:** Writing – review & editing, Writing – original draft, Validation, Methodology, Investigation, Formal analysis, Data curation, Conceptualization.

Declaration of Competing Interest

The authors declare that they have no known competing financial interests or personal relationships that could have appeared to influence the work reported in this paper.

Acknowledgement

The authors would like to acknowledge the support from Australian

Research Council (ARC), Australia (FT220100177, LP230100288, DP220101051, DP220100036 and IH200100010).

Appendix A. Supporting information

Supplementary data associated with this article can be found in the online version at doi:10.1016/j.nanoen.2024.110380.

Data Availability

Data will be made available on request.

References

[1] Z.L. Wang, From contact electrification to triboelectric nanogenerators, Rep. Prog. Phys. 84 (9) (2021) 096502.
[2] R. Zhang, H. Olin, Material choices for triboelectric nanogenerators: a critical review, EcoMat 2 (4) (2020) e12062.
[3] R. Walden, C. Kumar, D.M. Mulvihill, S.C. Pillai, Opportunities and challenges in triboelectric nanogenerator (TENG) based sustainable energy generation technologies: a mini-review, Chem. Eng. J. Adv. 9 (2022) 100237.
[4] Y. Pang, T. He, S. Liu, X. Zhu, C. Lee, Triboelectric nanogenerator-enabled digital twins in civil engineering infrastructure 4.0: a comprehensive review, Adv. Sci. 11 (20) (2024) 2306574.
[5] F. Qu, W. Li, W. Dong, V.W.Y. Tam, T. Yu, Durability deterioration of concrete under marine environment from material to structure: a critical review, J. Build. Eng. 35 (2021) 102074.
[6] M. Alexander, H. Beushausen, Durability, service life prediction, and modelling for reinforced concrete structures – review and critique, Cem. Concr. Res. 122 (2019) 17–29.
[7] M. Zameeruddin, K.K. Sangle, Review on Recent developments in the performance-based seismic design of reinforced concrete structures, Structures 6 (2016) 119–133.
[8] W. Kim, D. Kim, I. Tcho, J. Kim, M. Kim, Y. Choi, Triboelectric nanogenerator: structure, mechanism, and applications, ACS Nano 15 (1) (2021) 258–287.
[9] C. Wang, H. Guo, P. Wang, J. Li, Y. Sun, D. Zhang, An advanced strategy to enhance TENG output: reducing triboelectric charge decay, Adv. Mater. 35 (17) (2023) 2209895.
[10] G. Li, S. Wu, Z. Sha, L. Zhao, D. Chu, C.H. Wang, S. Peng, A triboelectric nanogenerator powered piezoresistive strain sensing technique insensitive to output variations, Nano Energy 108 (2023) 108185.
[11] H. Chen, Q. Lu, X. Cao, N. Wang, Z.L. Wang, Natural polymers based triboelectric nanogenerator for harvesting biomechanical energy and monitoring human motion, Nano Res. 15 (3) (2022) 2505–2511.
[12] W. Wang, A. Yu, X. Liu, Y. Liu, Y. Zhang, Y. Zhu, Y. Lei, M. Jia, J. Zhai, Z.L. Wang, Large-scale fabrication of robust textile triboelectric nanogenerators, Nano Energy 71 (2020) 104605.
[13] G. Li, S. Wu, Z. Sha, Y. Zhou, C.-H. Wang, S. Peng, Dual-breakdown direct-current triboelectric nanogenerator with synergistically enhanced performance, Nano Energy 99 (2022) 107355.
[14] H. Liu, Y. Feng, J. Shao, Y. Chen, Z.L. Wang, H. Li, X. Chen, Z. Bian, Self-cleaning triboelectric nanogenerator based on TiO2 photocatalysis, Nano Energy 70 (2020) 104499.
[15] W. Li, Y. Xiang, W. Zhang, K. Loos, Y. Pei, Ordered mesoporous SiO2 nanoparticles as charge storage sites for enhanced triboelectric nanogenerators, Nano Energy 113 (2023) 108539.
[16] W. Li, L. Lu, F. Yan, G. Palasantzas, K. Loos, Y. Pei, High-performance triboelectric nanogenerators based on TPU/mica nanofiber with enhanced tribo-positivity, Nano Energy 114 (2023) 108629.
[17] J. Chen, H. Guo, P. Ding, R. Pan, W. Wang, W. Xuan, X. Wang, H. Jin, S. Dong, J. Luo, Transparent triboelectric generators based on glass and polydimethylsiloxane, Nano Energy 30 (2016) 235–241.
[18] K. Scrivener, A. Ouzia, P. Juilland, A. Kunhi Mohamed, Advances in understanding cement hydration mechanisms, Cem. Concr. Res. 124 (2019) 105823.
[19] J.W. Bullard, H.M. Jennings, R.A. Livingston, A. Nonat, G.W. Scherer, J. S. Schweitzer, K.L. Scrivener, J.J. Thomas, Mechanisms of cement hydration, Cem. Concr. Res. 41 (12) (2011) 1208–1223.
[20] F. Sanchez, K. Sobolev, Nanotechnology in concrete – a review, Constr. Build. Mater. 24 (11) (2010) 2060–2071.
[21] R.D. Hooton, J.A. Bickley, Design for durability: the key to improving concrete sustainability, Constr. Build. Mater. 67 (2014) 422–430.
[22] W. Li, W. Dong, Y. Guo, K. Wang, S.P. Shah, Advances in multifunctional cementitious composites with conductive carbon nanomaterials for smart infrastructure, Cem. Concr. Compos. 128 (2022) 104454.
[23] W. Dong, W. Li, Z. Tao, K. Wang, Piezoresistive properties of cement-based sensors: Review and perspective, Constr. Build. Mater. 203 (2019) 146–163.
[24] W. Dong, W. Li, N. Lu, F. Qu, K. Vessalas, D. Sheng, Piezoresistive behaviours of cement-based sensor with carbon black subjected to various temperature and water content, Compos. Part B: Eng. 178 (2019) 107488.
[25] W. Dong, W. Li, K. Vessalas, X. He, Z. Sun, D. Sheng, Piezoresistivity deterioration of smart graphene nanoplate/cement-based sensors subjected to sulphuric acid attack, Composites, Communications 23 (2021) 100563.
[26] A. Mohammed, J.G. Sanjayan, W.H. Duan, A. Nazari, Graphene oxide impact on hardened cement expressed in enhanced freeze–Thaw resistance, J. Mater. Civ. Eng. 28 (9) (2016) 04016072.
[27] W. Dong, W. Li, K. Wang, B. Han, D. Sheng, S.P. Shah, Investigation on physicochemical and piezoresistive properties of smart MWCNT/cementitious composite exposed to elevated temperatures, Cem. Concr. Compos. 112 (2020) 103675.
[28] J. Luo, C. Zhou, W. Li, S. Chen, A. Habibnejad Korayem, W. Duan, Using graphene oxide to improve physical property and control ASR expansion of cement mortar, Constr. Build. Mater. 307 (2021) 125006.
[29] W. Long, Y. Gu, F. Xing, K.H. Khayat, Microstructure development and mechanism of hardened cement paste incorporating graphene oxide during carbonation, Cem. Concr. Compos. 94 (2018) 72–84.
[30] M. Jung, Y. Lee, S. Hong, J. Moon, Carbon nanotubes (CNTs) in ultra-high performance concrete (UHPC): Dispersion, mechanical properties, and electromagnetic interference (EMI) shielding effectiveness (SE), Cem. Concr. Res. 131 (2020) 106017.
[31] M. Lezgy-Nazargah, S. Saeidi-Aminabadi, M.A. Yousefzadeh, Design and fabrication of a new fiber-cement-piezoelectric composite sensor for measurement of inner stress in concrete structures, Arch. Civ. Mech. Eng. 19 (2) (2019) 405–416.
[32] W. Dong, W. Li, Y. Guo, F. Qu, K. Wang, D. Sheng, Piezoresistive performance of hydrophobic cement-based sensors under moisture and chloride-rich environments, Cem. Concr. Compos. 126 (2022) 104379.
[33] G. Karalis, J. Zhao, M. May, M. Liebscher, I. Wollny, W. Dong, T. Köberle, L. Tzounis, M. Kaliske, V. Mechtcherine, Efficient Joule heaters based on mineral-impregnated carbon-fiber reinforcing grids: An experimental and numerical study on a multifunctional concrete structure as an electrothermal device, Carbon 222 (2024) 118898.
[34] N. Chanut, D. Stefaniuk, J.C. Weaver, Y. Zhu, Y. Shao-Horn, A. Masic, F.-J. Ulm, Carbon–cement supercapacitors as a scalable bulk energy storage solution, Proc. Natl. Acad. Sci. 120 (32) (2023) e2304318120.
[35] S.I. Basha, S.S. Shah, S. Ahmad, M. Maslehuddin, M.M. Al-Zahrani, M.A. Aziz, Construction building materials as a potential for structural supercapacitor applications, Chem. Rec. 22 (11) (2022) e202200134.
[36] W. Li, W. Dong, S.P. Shah. Multifunctional Cement-Based Sensors for Intelligent Infrastructure: Design, Fabrication and Application, CRC Press, 2024.
[37] W. Li, Y. Guo, X. Zhang, W. Dong, X. Li, T. Yu, K. Wang, Development of self-sensing ultra-high-performance concrete using hybrid carbon black and carbon nanofibers, Cem. Concr. Compos. 148 (2024) 105466.
[38] B. Lei, L. Kong, Y. Guo, B. Sun, X. Li, K. Wu, V. Tam, W. Li, Optimizing decarbonation and sustainability of concrete pavement: A case study, Case Stud, Constr. Mater. (2024) e03574.
[39] N. Makul, Modern sustainable cement and concrete composites: Review of current status, challenges and guidelines, Sustain. Mater. Technol. 25 (2020) e00155.
[40] W. Borja, M. Adarmouch, Y. El Hafiane, Y. Daafi, Y. Tamraoui, J. Alami, Synthesis of nano-silica as a promising route of recycling phosphate waste rocks and its incorporation in mortars, Sustain. Mater. Technol. 37 (2023) e00684.
[41] W. Dong, W. Li, K. Wang, S.P. Shah, Physicochemical and Piezoresistive properties of smart cementitious composites with graphene nanoplates and graphite plates, Constr. Build. Mater. 286 (2021) 122943.
[42] G. Li, J. Zhang, F. Huang, S. Wu, C.-H. Wang, S. Peng, Transparent, stretchable and high-performance triboelectric nanogenerator based on dehydration-free ionically conductive solid polymer electrode, Nano Energy 88 (2021) 106289.
[43] W. Dong, W. Li, Z. Sun, I. Ibrahim, D. Sheng, Intrinsic graphene/cement-based sensors with piezoresistivity and superhydrophobicity capacities for smart concrete infrastructure, Autom. Constr. 133 (2022) 103983.
[44] N. Wang, Y. Zheng, Y. Feng, F. Zhou, D. Wang, Biofilm material based triboelectric nanogenerator with high output performance in 95% humidity environment, Nano Energy 77 (2020) 105088.
[45] Y. Hu, X. Wang, H. Li, H. Li, Z. Li, Effect of humidity on tribological properties and electrification performance of sliding-mode triboelectric nanogenerator, Nano Energy 71 (2020) 104640.
[46] W. Baomin, D. Shuang, Effect and mechanism of graphene nanoplatelets on hydration reaction, mechanical properties and microstructure of cement composites, Constr. Build. Mater. 228 (2019) 116720.
[47] F. Basquiroto de Souza, E. Shamsaei, K. Sagoe-Crentsil, W. Duan, Proposed mechanism for the enhanced microstructure of graphene oxide–Portland cement composites, J. Build. Eng. 54 (2022) 104604.
[48] Z. Bai, Y. Xu, Z. Zhang, J. Zhu, C. Gao, Y. Zhang, H. Jia, J. Guo, Highly flexible, porous electroactive biocomposite as attractive tribopositive material for advancing high-performance triboelectric nanogenerator, Nano Energy 75 (2020) 104884.
[49] S. Mishra, P. Supraja, D. Haranath, R.R. Kumar, S. Pola, Effect of surface and contact points modification on the output performance of triboelectric nanogenerator, Nano Energy 104 (2022) 107964.
[50] J. Sintusiri, V. Harnchana, V. Amornkitbamrung, A. Wongsa, P. Chindaprasirt, Portland Cement-TiO2 triboelectric nanogenerator for robust large-scale mechanical energy harvesting and instantaneous motion sensor applications, Nano Energy 74 (2020) 104802.
[51] S. Kuntharin, V. Harnchana, J. Sintusiri, P. Thongbai, A. Klamchuen, K. Sinthiptharakoon, V. Amornkitbamrung, P. Chindaprasirt, Smart triboelectric floor based on calcium silicate-carbon composite for energy harvesting and motion sensing applications, Sens. Appl., Sens. Actuators A: Phys. 358 (2023) 114423.
[52] J. Cao, D.D.L. Chung, Electric polarization and depolarization in cement-based materials, studied by apparent electrical resistance measurement, Cem. Concr. Res. 34 (3) (2004) 481–485.

[53] W. Dong, W. Li, X. Zhu, D. Sheng, S.P. Shah, Multifunctional cementitious composites with integrated self-sensing and hydrophobic capacities toward smart structural health monitoring, Cem. Concr. Compos. 118 (2021) 103962.
[54] X. Wang, S. Niu, F. Yi, Y. Yin, C. Hao, K. Dai, Y. Zhang, Z. You, Z.L. Wang, Harvesting ambient vibration energy over a wide frequency range for self-powered electronics, ACS Nano 11 (2) (2017) 1728–1735.
[55] L. Cheng, Q. Xu, Y. Zheng, X. Jia, Y. Qin, A self-improving triboelectric nanogenerator with improved charge density and increased charge accumulation speed, Nat. Commun. 9 (1) (2018) 3773.
[56] K. Zhao, W. Sun, S. Li, Z. Song, M. Zhong, D. Zhang, B.-N. Gu, M.-J. Liu, H. Fu, H. Liu, C. Meng, Y.-L. Chueh, Rational design on high-performance triboelectric nanogenerator consisting of silicon carbide@silicon dioxide nanowhiskers/polydimethylsiloxane (SiC@SiO2/PDMS) nanocomposite films, Discov. Nano 18 (1) (2023) 69.
[57] X. Chen, X. Wang, Triboelectric Nanogenerators as a High-Voltage Source, in: Z. L. Wang, Y. Yang, J. Zhai, J. Wang (Eds.), Handbook of Triboelectric Nanogenerators, Springer International Publishing, Cham, 2023, pp. 1–42.
[58] W. Dong, W. Li, K. Wang, Z. Luo, D. Sheng, Self-sensing capabilities of cement-based sensor with layer-distributed conductive rubber fibres, Sens. Actuators A: Phys. 301 (2020) 111763.
[59] Y. Ra, J.W. Kim, I. You, S. Jang, S. Cho, G. Gwon, D. Kam, D. Lee, A. Ahmad, M. R. Karim, S.-J. Lee, D. Choi, Direct electrospinning of reconstructable PVDF-TrFE nanofibrous mat onto conductive cement nanocomposite for triboelectricity-assisted net zero energy structure, Chem. Eng. J. 485 (2024) 149662.
[60] S. Wang, L. Lin, Z.L. Wang, Triboelectric nanogenerators as self-powered active sensors, Nano Energy 11 (2015) 436–462.
[61] J. Luo, Z.L. Wang, Recent progress of triboelectric nanogenerators: from fundamental theory to practical applications, EcoMat 2 (4) (2020) e12059.
[62] M. Seol, S. Lee, J. Han, D. Kim, G. Cho, Y. Choi, Impact of contact pressure on output voltage of triboelectric nanogenerator based on deformation of interfacial structures, Nano Energy 17 (2015) 63–71.
[63] P. Munirathinam, A. Anna Mathew, V. Shanmugasundaram, V. Vivekananthan, Y. Purusothaman, S.-J. Kim, A. Chandrasekhar, A comprehensive review on triboelectric nanogenerators based on real-time applications in energy harvesting and self-powered sensing, Mater. Sci. Eng. B 297 (2023) 116762.
[64] Q. Zhang, K. Barri, S.R. Kari, Z.L. Wang, A.H. Alavi, Multifunctional triboelectric nanogenerator-enabled structural elements for next generation civil infrastructure monitoring systems, Adv. Funct. Mater. 31 (47) (2021) 2105825.
[65] C. Chang, Y. Cheng, C. Ho, Surface engineering of a triboelectric nanogenerator for room temperature high-performance self-powered formaldehyde sensors, J. Mater. Chem. A 10 (42) (2022) 22373–22389.
[66] X. Li, X. Yin, W. Wang, H. Zhao, D. Liu, L. Zhou, C. Zhang, J. Wang, Carbon captured from vehicle exhaust by triboelectric particular filter as materials for energy storage, Nano Energy 56 (2019) 792–798.